16th Australasian Fluid Mechanics Conference
Crown Plaza, Gold Coast, Australia
2-7 December 2007

Sub-Filter Scale Models for Scalar Transport in Large Eddy Simulations

N. J. Williamson [1], M. P. Kirkpatrick[1], S. A. Armfield[1] and M. Behnia [2]

[1]Department of Aerospace, Mechanical and Mechatronic Engineering
The University of Sydney, NSW, 2006 AUSTRALIA

[2]Dean of Graduate Studies, The University of Sydney, NSW, 2006 AUSTRALIA

Abstract

Large eddy simulation (LES) of turbulent heat transfer in an infinite channel has been used to compare the performance of several promising sub-filter-scale models for modelling the transport of a passive scalar. The dynamic mixed model and the dynamic reconstruction model (a higher order version of the mixed model) have been reported in the literature to perform very well in LES of turbulent flow. Here these models are tested to determine the model's suitability for modelling transport of a passive scalar. These models together with the dynamic Smagorinsky model and a no-model case, are tested at a Prandtl number of 0.71 and Reynolds number of 180 based on wall friction velocity and channel half width. Both the dynamic reconstruction model and the dynamic mixed model perform very well showing clear improvement in the prediction of the mean flow and other turbulent statistics compared to the no-model case. The standard dynamic Smagorinsky model without the additional reconstruction terms performs quite poorly.

Introduction

In a large eddy simulation, a low pass filter is applied to the governing equations, separating the large resolved scales from the unresolved sub-filter-scales (SFS). In most LES simulations the computational grid and the discretisation of the equations provide the implicit filter, where the filter width is taken as being proportional to the grid dimensions.

There are several difficulties however with the implicit nature of the filter in these simulations. Firstly, with low order accuracy finite difference schemes, the implicit filtering is smooth, meaning it removes energy from the large resolved scales as well as the small scales [3]. The energy removed from the large scales then needs to be reconstructed by the SFS model. When only an implicit filter is used, the shape of the filter is unknown making this reconstruction difficult. Secondly, unless high order finite differencing schemes are used, the numerical error in the small resolved scales is significant. It has been long known that using a grid size smaller than an explicitly applied filter would provide a means of reducing the numerical error in the smallest resolved scales. Recent work has suggested revisiting these ideas [1, 2].

Carati *et al.* [4] illustrate how combined discretisation — implicit filtering (denoted by an operator $\tilde{G}$) and explicit filtering (denoted by the operator $\bar{G}$) — affects the decomposition of the velocity field. The authors re-write the governing equations to distinguish between the explicit filtering and discretisation operations as follows,

$$\frac{\partial \overline{\tilde{u}}_i}{\partial x_i} = 0, \tag{1}$$

$$\frac{\partial \overline{\tilde{u}}_i}{\partial t} + \frac{\partial (\widetilde{\overline{\tilde{u}}_i \overline{\tilde{u}}_j})}{\partial x_j} = -\frac{\partial \overline{\tilde{p}}}{\partial x_i} + \nu \frac{\partial^2 \overline{\tilde{u}}_i}{\partial x_j \partial x_j} - \frac{\partial \widetilde{\tau_{ij}}}{\partial x_j}, \tag{2}$$

where $\tau_{ij} = \overline{(u_i u_j)} - (\overline{\tilde{u}}_i \overline{\tilde{u}}_j)$. Carati *et al.* [4] proposed that the residual stresses from equation (2) could be decomposed to $\tau_{ij} = \tau_{RSFS} + \tau_{SGS}$ where $\tau_{SGS} = (\overline{u_i u_j} - \overline{\tilde{u}_i \tilde{u}_j})$ and $\tau_{RSFS} = (\overline{\tilde{u}_i \tilde{u}_j} - \bar{\tilde{u}}_i \bar{\tilde{u}}_j)$. τ_{SGS} is the sub grid scale (SGS) stress that cannot be captured by the grid or implicit filter. τ_{RSFS} represents the interactions of the resolved scales ($\bar{\tilde{u}}$) and SFS motions ($\tilde{u} - \bar{\tilde{u}}$), which are the filtered scales that are still supported by the grid.

These ideas have been successfully applied to several LES simulations of turbulent flow. Winckelmans *et al.* [6] formulated a dynamic reconstruction model (DRM) based on the explicit filtering framework they introduced. Gullbrand and Chow [7] implemented a higher order version of the reconstruction model and found improved performance over the dynamic mixed model (DMM) of Zang *et al.* [8] and the dynamic Smagorinsky model (DSM) of Germano *et al.* [9] in a turbulent channel flow simulation. Gullbrand and Chow formulated the SFS stress as follows, $\tau_{RSFS} = \overline{(\tilde{u}_i^\star \tilde{u}_j^\star)} - (\bar{\tilde{u}}_i \bar{\tilde{u}}_j)$ and $\tau_{SGS} = -2c_s(\tilde{\Delta})^2 |\bar{\tilde{S}}| \bar{\tilde{S}}_{ij}$, where $\tilde{u}_i^\star$ is an approximation of $\tilde{u}_i$ found using,

$$\tilde{u}_i \approx \tilde{u}_i^\star = \sum_{n=0}^{N} (I - \bar{G})^n \overline{\tilde{u}}_i. \tag{3}$$

In this way, the model is simply a higher order version of the dynamic mixed model of Zang *et al.* [8], where $\tilde{u}$ in the τ_{RSFS} term is approximated by $\bar{\tilde{u}}$ instead of $u^\star$. Chow *et al.* [5] applied the DRM to an atmospheric boundary layer simulation and found improved performance compared with DSM and DMM models.

In this study the interest is in determining how the DRM model performs when applied to turbulent transport of a passive scalar.

Much of the development in SFS heat flux models has followed directly from models of the residual stress tensor in the momentum equations. The dynamic heat flux model proposed by Moin *et al.* [10] is based on the dynamic Smagorinsky model of Germano *et al.* [9]. The SFS heat flux (γ_j) is modelled using, $\gamma_j = -c_\theta \tilde{\Delta}^2 |\tilde{S}| \frac{\partial \tilde{\theta}}{\partial x_j}$, where the model coefficient c_θ is calculated dynamically. Following this work a number of researchers have proposed non-linear models for the SFS heat flux term, which removes the assumption of alignment with the resolved temperature gradient. Salvetti and Banerjee [11] developed a dynamic two parameter model (DTM) which is similar to DMM of Zhang *et al.* [8]. In *a priori* tests the authors found both DMM and DTM had a high degree of correlation with DNS data for both heat flux and SFS stresses, while DSM was less satisfactory. Jiménez *et al.* [12] tested DMM, DTM and DSM in a mixing layer and found that the eddy diffusivity model works well, provided the resolved velocity field is captured well. In *a posteriori* tests, the authors found comparable results when DSM was used for modelling γ_j and DMM used for modelling τ_{ij} and when DMM was used for both γ_j and τ_{ij}. The results were not as good when DSM was used for modelling both γ_j and τ_{ij}.

Peng and Davidson [13] developed a tensor diffusivity model which formulates $\gamma_j \propto -S_{ij} \partial\theta / \partial x_j$. Yin *et al.* [14] applied this model in a simulation of turbulent channel flow with buoyancy.

The authors found better agreement with DNS using the tensor diffusivity model for γ_j and a non linear model for τ_{ij}, than using DSM for both γ_j and τ_{ij}. Wang *et al.* [15] developed a tensorial diffusivity model which the authors demonstrate is a more general case of the two coefficient dynamic mixed model of Sarghini *et al.* [16]. The model showed slightly improved performance over DSM in a simulation of turbulent channel flow.

The mixed models appear attractive both from the point of view of the framework outlined by Carati *et al.* [4] and also from a physical standpoint. In *a priori* tests, the mixed models show stronger correlation with DNS results than models without the τ_{RSFS} term [11]. In *a postiori* tests the mixed models have performed well in many test cases [7, 8, 16, 17] and have been the subject of continued interest and development. The reported good performance of the mixed models for both SFS residual stress and SFS heat flux is encouraging and suggests that DRM, which is a higher order version of DMM, should also perform well. In this study we compare the performance of DRM, DMM and DSM for both SFS heat flux and SFS stress in a simulation of turbulent channel flow with transport of a passive scalar. Two aspects are of particular interest. Firstly, how the closure of the SFS stress term τ_{ij} affects both the flow and the transport of the scalar and secondly, how the closure of the SFS heat flux term γ_j performs.

Governing Equations

The models are tested in a fully developed turbulent channel flow simulation between two parallel vertical walls. The streamwise (x) and spanwise directions (z) have periodic boundaries while no slip boundary conditions are used at the channel walls. The flow is driven by a constant mean pressure gradient, which becomes unity when the flow variables are nondimensionalised by the wall friction velocity $u_\tau = \sqrt{\tau_w/\rho}$, and the channel half width δ. The filtered conservation of mass and momentum equations are given in equation (1) and (2) respectively. The configuration tested is for channel flow with constant heat flux at the walls. Buoyancy is not considered so temperature becomes a passive scalar. The statistically averaged temperature increases linearly with respect to x. The instantaneous temperature T, can be divided into the fluctuating component θ and the mean component as follows,

$$T(x,y,z) = \frac{d\langle T_m\rangle}{dx} - \theta(x,y,z), \tag{4}$$

where the mean component is found from an average across the channel section,

$$\langle T_m\rangle = \int_0^1 \bar{u}_1 \bar{T}\, dy \Bigg/ \int_0^1 \bar{u}_1\, dy, \tag{5}$$

In this equation $\bar{()}$ indicates statistical average in time. For channel flow the streamwise temperature gradient is,

$$\frac{d\langle T_m\rangle}{dx} = \frac{1}{\langle u\rangle}, \tag{6}$$

where $\langle u\rangle$ is the time averaged velocity, averaged over the channel section. With this substitution, the equation for the transport of the passive scalar becomes,

$$\frac{\partial\bar{\bar{\theta}}}{\partial t} + \frac{\partial(\widetilde{\bar{\bar{\theta}}\bar{\bar{\tilde{u}}}_j})}{\partial x_j} = \frac{\nu}{Pr}\frac{\partial^2\bar{\bar{\theta}}}{\partial x_j\partial x_j} - \frac{\partial\tilde{\gamma}}{\partial x_j} + \frac{u_1}{\langle u\rangle}, \tag{7}$$

where, $\gamma = \overline{(\theta u_j)} - (\bar{\tilde{\theta}}\bar{\tilde{u}}_j)$. At the walls, the following boundary conditions are enforced, $u = 0$, $\theta = 0$ at $y = 0$ and $y = 2\delta$.

SFS Models

Three SFS models are compared in this study, the dynamic Smagorinsky model (DSM) of Germano *et al.* [9], the dynamic mixed model (DMM) of Vreman *et al.* [17] and the dynamic reconstruction model (DRM) of Gullbrand and Chow [7].

The dynamic Smagorinsky model is formulated as $\tau_{ij} = -2c_s(\tilde{\Delta})^2|\tilde{S}|\tilde{S}_{ij}$ where the model coefficient and length scale $c_s(\Delta)^2$ are calculated dynamically [9]. There is no explicit filtering in the DSM model and $\tau_{RSFS} = 0$. The DMM model SFS term is formulated as,

$$\tau_{ij} = (\overline{\bar{\tilde{u}}_i\bar{\tilde{u}}_j}) - (\bar{\bar{\tilde{u}}}_i\bar{\bar{\tilde{u}}}_j) - 2c_s(\tilde{\Delta})^2|\bar{\tilde{S}}|\bar{\tilde{S}}_{ij}. \tag{8}$$

To formulate the dynamic model coefficient $c_s(\tilde{\Delta})^2$, the equations are filtered to the $\hat{\bar{\bar{\tilde{u}}}}$ level as follows,

$$\frac{\partial\hat{\bar{\bar{\tilde{u}}}}_i}{\partial t} + \frac{\partial(\widetilde{\hat{\bar{\bar{\tilde{u}}}}_i\hat{\bar{\bar{\tilde{u}}}}_j})}{\partial x_j} = -\frac{\partial\hat{\bar{\bar{\tilde{p}}}}}{\partial x_i} + \frac{1}{Re_\tau}\frac{\partial^2\hat{\bar{\bar{\tilde{u}}}}_i}{\partial x_j\partial x_j} - \frac{\partial\widetilde{T_{ij}}}{\partial x_j}, \tag{9}$$

where $T_{ij} = \widehat{\overline{(u_iu_j)}} - (\hat{\bar{\bar{\tilde{u}}}}_i\hat{\bar{\bar{\tilde{u}}}}_j)$. The expression for L_{ij} is given as,

$$L_{ij} = T_{ij} - \widehat{\tau}_{ij} = (\widehat{\bar{\tilde{u}}_i\bar{\tilde{u}}_j}) - (\hat{\bar{\tilde{u}}}_i\hat{\bar{\tilde{u}}}_j). \tag{10}$$

At the test level, the model for T_{ij} can be written as,

$$T_{ij} = (\widehat{\overline{\hat{\bar{\tilde{u}}}_i\hat{\bar{\tilde{u}}}_j}}) - (\hat{\bar{\hat{\bar{\tilde{u}}}}}_i\hat{\bar{\hat{\bar{\tilde{u}}}}}_j) - 2c_s(\hat{\Delta})^2|\hat{\bar{\tilde{S}}}|\hat{\bar{\tilde{S}}}_{ij}. \tag{11}$$

Combining equations (8) and (11) using the definition for L_{ij} gives,

$$\begin{aligned} L_{ij} &= T_{ij} - \widehat{\tau}_{ij}, \\ &= (\widehat{\overline{\hat{\bar{\tilde{u}}}_i\hat{\bar{\tilde{u}}}_j}}) - (\hat{\bar{\hat{\bar{\tilde{u}}}}}_i\hat{\bar{\hat{\bar{\tilde{u}}}}}_j) - 2c_s(\hat{\Delta})^2|\hat{\bar{\tilde{S}}}|\hat{\bar{\tilde{S}}}_{ij} \\ &- (\widehat{\overline{\bar{\tilde{u}}_i\bar{\tilde{u}}_j}} - \widehat{\bar{\bar{\tilde{u}}}_i\bar{\bar{\tilde{u}}}_j}) - 2c_s(\tilde{\Delta})^2\widehat{|\bar{\tilde{S}}|\bar{\tilde{S}}_{ij}}. \end{aligned} \tag{12}$$

Equating equation (10) and equation (12) gives,

$$L_{ij} - H_{ij} = 2c_s(\tilde{\Delta})^2M_{ij}, \tag{13}$$

where,

$$H_{ij} = \widehat{\overline{\hat{\bar{\tilde{u}}}_i\hat{\bar{\tilde{u}}}_j}} - \hat{\bar{\hat{\bar{\tilde{u}}}}}_i\hat{\bar{\hat{\bar{\tilde{u}}}}}_j - (\widehat{\overline{\bar{\tilde{u}}_i\bar{\tilde{u}}_j}} - \widehat{\bar{\bar{\tilde{u}}}_i\bar{\bar{\tilde{u}}}_j}), \tag{14}$$

and M_{ij} is given by,

$$M_{ij} = -\sigma^2|\hat{\bar{\tilde{S}}}|\hat{\bar{\tilde{S}}}_{ij} + \widehat{|\bar{\tilde{S}}|\bar{\tilde{S}}_{ij}}, \tag{15}$$

with $\sigma = \hat{\bar{\tilde{\Delta}}}/\bar{\tilde{\Delta}}$. The dynamic model coefficient is defined as,

$$c_s(\tilde{\Delta})^2 = \frac{\langle M_{ij}(L_{ij} - H_{ij})\rangle}{2\langle M_{kl}M_{kl}\rangle}. \tag{16}$$

Here $\langle\rangle$ indicates a local averaging operation using the test filter $\hat{G}$. The scalar model is formulated similarly using,

$$\gamma = (\overline{\bar{\tilde{\theta}}\bar{\tilde{u}}_j}) - (\bar{\bar{\tilde{\theta}}}\bar{\bar{\tilde{u}}}_j) - c_\theta\tilde{\Delta}^2|\bar{\tilde{S}}|\frac{\partial\bar{\tilde{\theta}}}{\partial x_j}, \tag{17}$$

and the model coefficients are calculated using,

$$c_\theta(\Delta)^2 = -\frac{\langle F_j(E_j - G_j)\rangle}{\langle F_kF_k\rangle}, \tag{18}$$

$$G_j = \widehat{\overline{\hat{\bar{\tilde{\theta}}}\hat{\bar{\tilde{u}}}_j}} - \hat{\bar{\hat{\bar{\tilde{\theta}}}}}\hat{\bar{\hat{\bar{\tilde{u}}}}}_j - (\widehat{\overline{\bar{\tilde{\theta}}\bar{\tilde{u}}_j}} - \widehat{\bar{\bar{\tilde{\theta}}}\bar{\bar{\tilde{u}}}_j}). \tag{19}$$

In the DRM, the residual stress is constructed as:

$$\tau_{ij} = \overline{(\tilde{u}_i^\star \tilde{u}_j^\star)} - (\bar{\tilde{u}}_i \bar{\tilde{u}}_j) - 2c_s(\tilde{\Delta})^2 |\bar{\tilde{S}}| \bar{\tilde{S}}_{ij}, \tag{20}$$

where $\tilde{u}_i^\star$ is approximated using equation (3). To satisfy similarity of the SFS model at the test level, T_{ij} must also be reconstructed to below the filter level by the same degree. At the test level, reconstruction may be interpreted as the inverse filtering of $\hat{G}$. Assuming perfect reconstruction, this may be represented by the removal of a filter $\hat{G}$. In this case T_{ij} may be written as,

$$T_{ij} = (\widehat{\bar{\tilde{u}}_i \bar{\tilde{u}}_j}) - (\hat{\bar{\tilde{u}}}_i \hat{\bar{\tilde{u}}}_j) - 2c_s(\hat{\tilde{\Delta}})^2 |\hat{\bar{\tilde{S}}}| \hat{\bar{\tilde{S}}}_{ij}. \tag{21}$$

When combined with the Germano identity following the same approach as with the DMM, the model coefficient can be obtained as,

$$c_s(\bar{\tilde{\Delta}})^2 = \frac{\langle M_{ij}(L_{ij} - H_{ij})\rangle}{\langle M_{kl} M_{kl}\rangle}, \tag{22}$$

where $H_{ij} = (\widehat{\bar{\tilde{u}}_i \bar{\tilde{u}}_j}) - (\hat{\bar{\tilde{u}}}_i \hat{\bar{\tilde{u}}}_j) - (\widehat{\tilde{u}_i^\star \tilde{u}_j^\star} - \widehat{\bar{\tilde{u}}_i \bar{\tilde{u}}_j})$. The scalar SFS model is formulated in a similar manner with,

$$\gamma = \overline{(\tilde{\theta}^\star \tilde{u}_j^\star)} - (\bar{\tilde{\theta}} \bar{\tilde{u}}_j) - 2c_\theta(\tilde{\Delta})^2 |\bar{\tilde{S}}| \frac{\partial \bar{\tilde{\theta}}}{\partial x_j}. \tag{23}$$

In all simulations in this study, explicit filtering is only applied in the SFS models, the velocity field itself is not filtered.

Numerical Procedure

The filtered equations are solved within a finite volume code on a staggered Cartesian grid. Second-order central differencing has been used for the spatial discretisation on all terms in the momentum and pressure correction equation. A fractional step method is used to advance the solution in time with the advective terms integrated using a second order Adams-Bashforth scheme and the diffusive terms using a second order accurate Crank-Nicolson scheme. The PUFFIN code is described more completely in [18].

The simulations have been chosen to match DNS results of Abe *et al.* [19] at $Re_\tau = u_\tau \delta/\nu = 180$ and $Pr = 0.71$. The domain size is $L_x = 12.8$, $L_y = 2.0$ and $L_z = 6.4$ with the number of nodes in each direction, $n_x = 64$, $n_y = 74$ and $n_z = 64$. The cell sizes in wall units are $\Delta x^+ = 36$, $\Delta z^+ = 18$, $\Delta y^+_{min} = 0.7$, $\Delta y^+_{max} = 15.3$. Constant linear stretching is used in the wall normal direction (y) while a uniform mesh is used in the homogeneous directions (x, z). In this study the test and explicit filters are only applied in $x-z$ plane. A discrete two dimensional filter can be written as,

$$\overline{G}(i, j) = a(m)a(n)f(i+m, j+n). \tag{24}$$

The filter coefficients $a(m)$ and $a(n)$ need to be specified. In this study, the filters of Zang *et al.* [8] have been used where, the filter $\bar{G}$ has coefficients $a(-1) = 0.125$, $a(0) = 0.75$, $a(1) = 0.125$, and the test filter $\hat{G}$ has coefficients $a(-1) = 0.25$, $a(0) = 0.5$, $a(1) = 0.25$.

The order of reconstruction in the DRM is been set at $N = 5$ in equation (3). Initial tests have shown that increasing the level of reconstruction to $N = 10$, produces little change in the results.

In all simulations the time step was monitored so that the CFL number ($CFL = \Delta t u_i/\Delta x_i$) was maintained between $0.3 - 0.4$. Simulations were run until a statistically stationary solution was obtained which, for most simulations was ~ 30 non-dimensional time units (tu_τ/δ). Statistics were then collected over a further 15 non-dimensional time units.

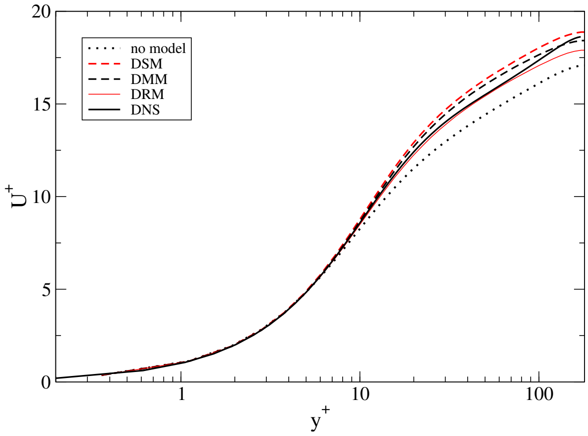

Figure 1: Mean streamwise velocity profile

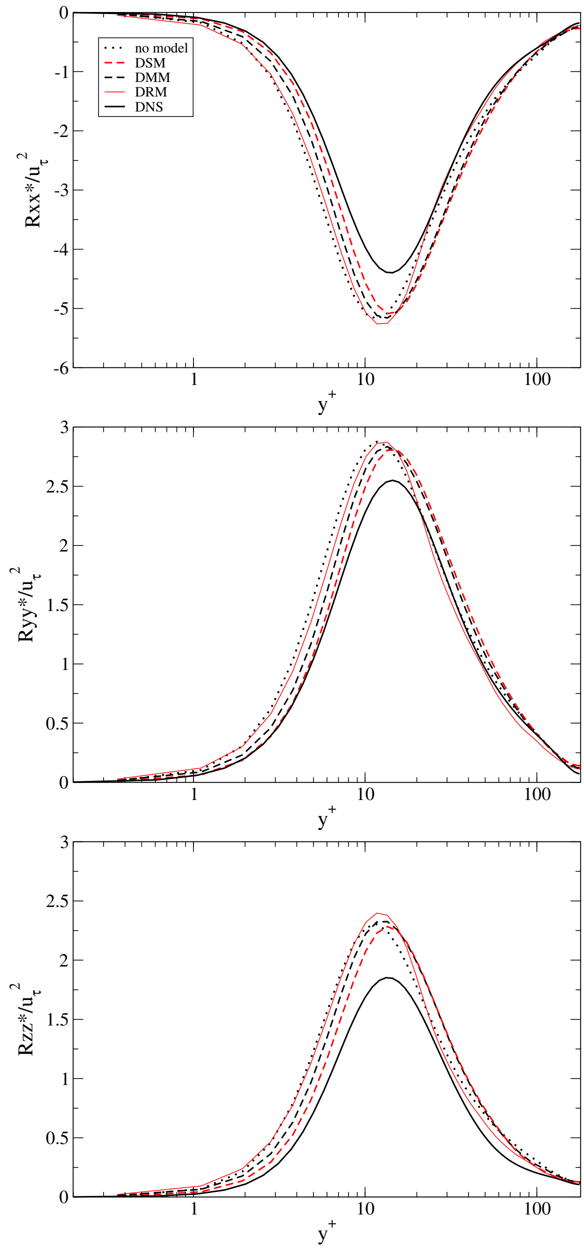

Figure 2: Traceless normal Reynolds stresses

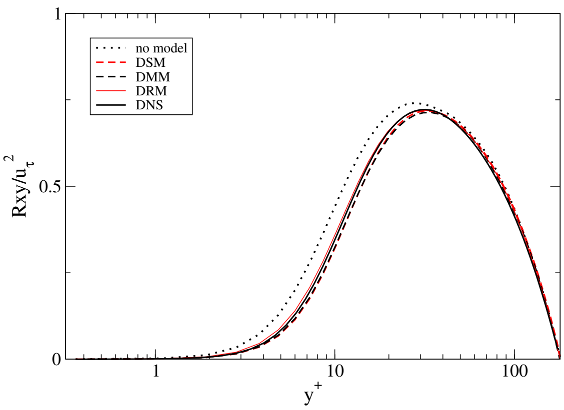

Figure 3: Total Reynolds stress R_{xy}

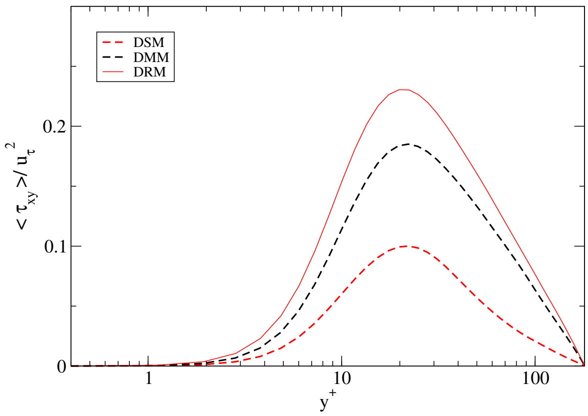

Figure 4: Model subgrid scale shear stress τ_{xy}

Results and discussion

The mean streamwise velocity is shown in figure 1 where $U^+ = \langle u^+ \rangle$ is given in wall units (where $u^+ = u/u_\tau$, and $y^+ = yu_\tau/\nu$). The mean velocity profiles are generally well captured, with DMM and DRM performing better than DSM. In the centre of the channel where the grid resolution is poorest, DRM is less accurate than DMM. DSM is too dissipative over the entire range. Outside the log-law region ($y^+ > 70$), DRM underpredicts the mean velocity. DRM appears to be applying insufficient dissipation at the channel centre. This may be a low Reynolds number effect.

The traceless normal stresses R^*_{xx}, R^*_{yy} and R^*_{zz}, are compared in figure 2. They are calculated as, $-R_{xx} = \langle u'u' \rangle - \langle \tau_{xx} \rangle$, where $\langle\rangle$ indicates an average over the $x-z$ plane and time. The trace is subtracted following, $R^*_{xx} = R_{xx} - 1/3(R_{xx} + R_{yy} + R_{zz})$. This is important because the dynamic Smagorinsky component of the models provides no model for the trace and thus the normal stresses cannot be compared directly with DNS results unless the trace is removed [6]. It is also important to include the model component, as this can be significant in the models with the τ_{RSFS} term such as DRM or DMM. Gullbrand and Chow [7] did not include the model component in their comparison and came to the conclusion that the normal stresses were dramatically better predicted by DMM and DRM. In fact, the resolved component is simply reduced in these models as the SFS model contributes more. Including the effect of the SFS model as in figure 2, shows that the predicted normal stresses are similar with all models.

The shear stress R_{xy} is shown in figure 3. This is calculated

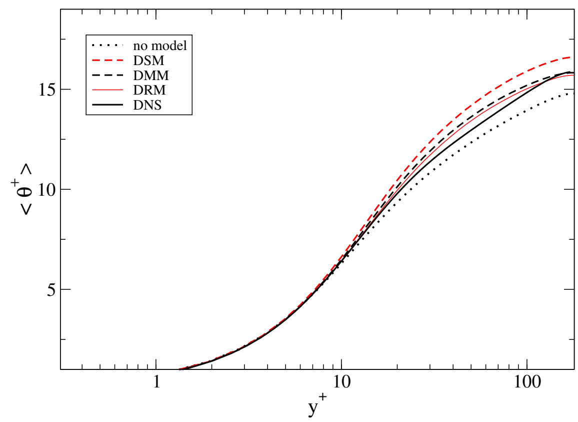

Figure 5: Mean temperature profile in wall units

as $R_{xy} = -\langle u'v' \rangle - \langle \tau_{xy} \rangle$, where u' is the fluctuating resolved velocity component calculated using, $u = \langle u \rangle + u'$ and τ_{xy} is the model component. The shear stress is well predicted by all models, with clear improvements over the no-model case. DRM performs slightly better than DSM in the buffer layer region for $y^+ < 20$. The model component for the shear stress, τ_{xy}, is shown in figure 4. It is much greater for both DMM and DRM. This is expected because the explicit filtering means that the model represents a greater part of the spectrum.

The mean temperature profile is given in figure 5, non-dimensionalised by wall friction temperature, $\langle \theta^+ \rangle = \langle \theta \rangle / T_\tau$ where $T_\tau = q_w / \rho c_p u_\tau$. The predictions of the temperature profile are similar to those of the velocity profile. Both DRM and DMM capture the behaviour better than the DSM. DRM does not offer much improvement over DMM. None of the models capture the shape of the curve well in the log-law region ($y^+ \sim 20-70$).

The scalar flux from the walls h_y, is calculated as $h_y = \langle v'\theta' \rangle / u_\tau T_\tau + \langle \gamma_y \rangle / u_\tau T_\tau$. The results are given in figure 6 (a), with the model component given in figure 6 (b). Again, there are clear improvements over the no-model case. DMM, DRM and DSM all perform well. DRM and DMM are perhaps slightly better than DSM for $y^+ < 20$. The model component γ_y behaves in a similar manner to τ_{xy}, with its value much lower in the DSM simulation than with DRM and DMM.

Further tests have been conducted comparing the models performance in channel flow with constant temperature difference between the walls at $Re_\tau = 150$. The performance of the models is similar to that in the isoflux case tested here.

Conclusions

Several Large Eddy Simulation models have been examined within the framework of explicit filtering and reconstruction outlined by Carati *et al.* [4]. The dynamic mixed and dynamic reconstruction models have been applied to the simulation of transport of a passive scalar in a turbulent channel flow. For the prediction of the turbulent stresses and the mean flow statistics, all the models perform better than the no-model simulation. Both DMM and DRM perform better than DSM for most of the quantities examined, particularly in the buffer region and through most of the log-law region. DRM appears to offer some improvement over DMM, but overall the results are mixed. DRM underpredicts the mean velocity in the centre of the channel. The mean temperature and heat flux are generally well predicted. DRM appears to perform slightly better than DMM and DSM in the region close to the wall. The scalar flux

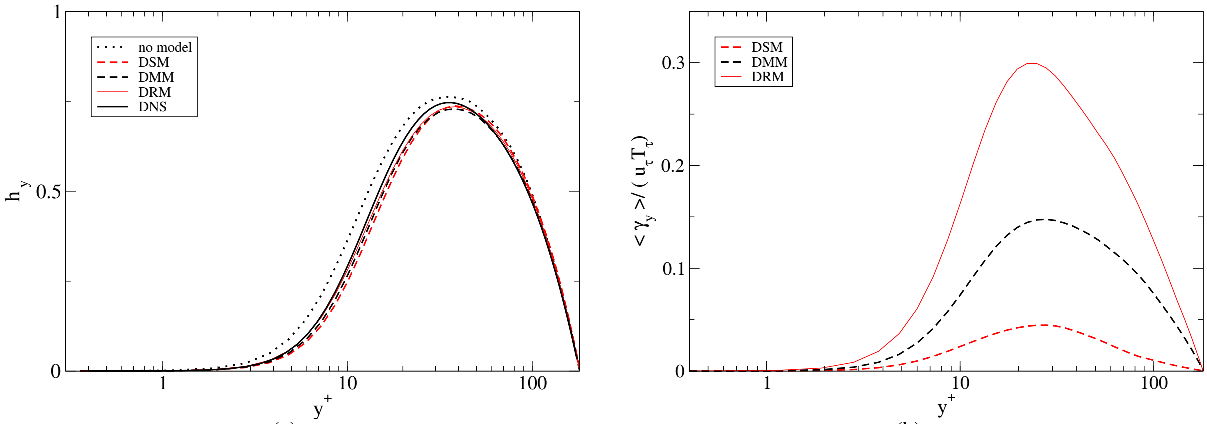

(a) (b)

Figure 6: Resolved and modelled temperature flux from the wall (a) and model subgrid heat flux h_y (b)

from the wall was quite well predicted by DRM and DMM for $y^+ < 20$. The no-model and DSM simulations were less accurate in this region.

Overall, DRM and DMM are promising concepts, for both the scalar SGS model and the residual stress. For most of the statistics examined, both models perform better than DSM. In several of the statistics examined however, their performance was mixed, so more work is needed before they can be trusted in more difficult simulations. Further tests are needed at higher Reynolds number to confirm these results.

References

[1] Brandt, T., A priori tests on numerical errors in large eddy simulation using finite differences and explicit filtering, *Int. J. Numer. Meth. in Fluids*, **51**, 2006, 635–657.

[2] Lund, T.S. and Kaltenbach, H.J., Experiments with explicit filtering for LES using a finite-difference method, *Annual Research Briefs*, Center for Turbulence Research NASA Ames-Stanford University, 1995, 91–105.

[3] De Stefano, G. and Vasilyev, O.V., ”Perfect” modeling framework for dynamic SGS model testing in large eddy simulation, *Theoret. Comput. Fluid Dynamics* , **18**, 2004, 27–41.

[4] Carati, D., Winckelmans, G.S. and Jeanmart, H., On the modelling of the subgrid-scale and filtered-scale stress tensors in large-eddy simulation, *J. Fluid Mech.*, **441**, 2001, 119–138.

[5] Chow, F.K., Street, R.L., Xue, M. and Ferziger, J.H., Explicit Filtering and Reconstruction Turbulence Modeling for Large-Eddy Simulation of Neutral Boundary Layer Flow, *J. Atmos. Sci.*, **62**, 2058–2077.

[6] Winckelmans, G.S., Wray, A.A., Vasilyev, O.V. and Jeanmart, H., Explicit-filtering large eddy simulation using the tensor-diffusivity model supplemented by a dynamic Smagorinsky term, *Phys. Fluids*, **13** , 2001, 1385–1403.

[7] Gullbrand, J. and Chow, F.K.. The effect of numerical errors and turbulence models in large-eddy simulations of channel flow, with and without explicit filtering, *J. Fluid Mech.*, **495**, 2003, 323–341.

[8] Zang, Y., Street, R.L. and Koseff, J.R., A dynamic mixed subgrid-scale model and its application to turbulent recirculating flows, *Phys. Fluids A*, **5**, 1993, 3186–3196.

[9] Germano, M., Piomelli, U., Moin, P. and Cabot, W.H., A dynamic subgrid-scale stress model, *Phys. Fluids A*, **3**, 1991, 1760–1765.

[10] Moin, P., Squires, K., Cabot, W. and Lee, S. A dynamic subgrid-scale model for compressible turbulence and scalar transport, *Phys. Fluids A*, **3**, 1991, 2746–2757.

[11] Salvetti, M.V. and Banerjee, S., A priori tests of a new dynamic subgrid-scale model for finite-difference large-eddy simulations, *Phys, of Fluids*, **7**, 1995, 2831–2847.

[12] Jimenez, C., Valino, L. and Dopazo, C., A priori and a posteriori tests of subgrid scale models for scalar transport *Phys. of Fluids*, **13**, 2001, 2433–2436.

[13] Peng, S.H. and Davidson, L., On a Subgrid-Scale Heat Flux Model for Large Eddy Simulation of Turbulent Thermal Flow, *Int. J. Heat Mass Tran.*, **45**, 2002, 1393–1405.

[14] Yin, J., Wang, B.C. and Bergstrom D.J.,Large-eddy simulation of combined forced and natural convection in a vertical plane channel, *Int. J. Heat Mass Tran.*, **50**, 2007, 3848–3861.

[15] Wang, B.C., Yee, E., Yin, J. and Bergstrom D.J., A general dynamic linear tensor-diffusivity subgrid-scale heat flux model for large-eddy simulation of turbulent thermal flows, *Numer, Heat Tr B-Fund*, **51**, 2007, 205–227.

[16] Sarghini, F., Piomelli, U. and Balaras, E., Scale-similar models for large-eddy simulations, *Phys. of Fluid*, **11**, 1999, 1596–1607.

[17] Vreman, B., Geurts, B. and Kuerten, H., Large-eddy simulation of the turbulence mixing layer, *J. Fluid Mech.*, **339**, 1997, 357–390.

[18] Kirkpatrick, M.P., Armfield, S.W. and Kent J.H., A representation of curved boundaries for the solution of the Navier-Stokes equations on a staggered three-dimensional Cartesian grid, *J. Comput. Phys.*, **184**, 2003, 1–36.

[19] Abe, H., Kawamura, H. and Matsuo, Y., Direct numerical simulation of a fully developed turbulent channel flow with respect to Reynolds number dependence, *J. Fluid. Eng-T. ASME*, **123**, 2001, 382–393.